

Compositional splines for representation of density functions

J. Machalová^a, R. Talská^{a*}, K. Hron^a, A. Gába^b

^aDepartment of Mathematical Analysis and Applications of Mathematics,
Faculty of Science, Palacký University Olomouc,
17. listopadu 12, CZ-77146 Olomouc, Czech Republic

^bDepartment of Natural Sciences in Kinanthropology,
Faculty of Physical Culture, Palacký University Olomouc,
tř. Míru 117, CZ-77111 Olomouc, Czech Republic

*Corresponding author. Email: talskarenata@seznam.cz

December 19, 2019

Abstract

In the context of functional data analysis, probability density functions as non-negative functions are characterized by specific properties of scale invariance and relative scale which enable to represent them with the unit integral constraint without loss of information. On the other hand, all these properties are a challenge when the densities need to be approximated with spline functions, including construction of the respective spline basis. The Bayes space methodology of density functions enables to express them as real functions in the standard L^2 space using the centered log-ratio transformation. The resulting functions satisfy the zero integral constraint. This is a key to propose a new spline basis, holding the same property, and consequently to build a new class of spline functions, called compositional splines, which can approximate probability density functions in a consistent way. The paper provides also construction of smoothing compositional splines and possible orthonormalization of the spline basis which might be useful in some applications. Finally, statistical processing of densities using the new approximation tool is demonstrated in case of simplicial functional principal component analysis with anthropometric data.

Keywords: spline representation, spline with zero integral, compositional spline, smoothing spline, simplicial functional principal component analysis

1 Introduction

Probability density functions are popularly known as non-negative functions satisfying the unit integral constraint. This clearly inhibits their direct processing using standard methods of functional data analysis [18] since unconstrained functions are assumed there. The same holds also for approximation of the raw input data using splines which is commonly considered to be a key step in functional data analysis. But more severely, in addition to the apparent unit integral constraint of densities which might seem to represent just a kind of numerical obstruction, density functions are rather characterized by deeper geometrical properties that need to be taken into account for any reliable analysis [6, 21, 22]. Specifically, in contrast to functions in the standard L^2 space, densities obey the scale invariance and relative scale properties [9]. Scale invariance means that not just the representation of densities with the unit integral constraint, but any its positive multiple conveys the same information about relative contributions of Borel sets on the whole probability mass. Relative scale can be explained directly with an example: the relative increase of a probability over a Borel set from 0.05 to 0.1 (2 multiple) differs from the increase 0.5 to 0.55 (1.1 multiple), although the absolute differences are the same in both cases. If we restrict to a bounded support $I = [a, b] \subset \mathbb{R}$ that is mostly used in practical applications [3, 9, 14, 15], density functions can be represented with respect to Lebesgue reference measure using the Bayes space $\mathcal{B}^2(I)$ of functions with square-integrable logarithm [6, 22].

The Bayes space $\mathcal{B}^2(I)$ has structure of separable Hilbert space that enables construction of an isometric isomorphism between $\mathcal{B}^2(I)$ and $L^2(I)$, the L^2 space restricted to I . Accordingly, analogies of summing two functions and multiplication of a function by a real scalar in the L^2 space together with an inner product between two densities are required. Given two absolutely integrable density functions $f, g \in \mathcal{B}^2(I)$ and a real number $\alpha \in \mathbb{R}$ we indicate with $f \oplus g$ and $\alpha \odot f$ the *perturbation* and *powering* operations, defined as

$$(f \oplus g)(x) = \frac{f(x)g(x)}{\int_I f(y)g(y) dy}, \quad (\alpha \odot f)(x) = \frac{f(x)^\alpha}{\int_I f(y)^\alpha dy}, \quad x \in I, \quad (1)$$

respectively. The resulting functions are readily seen to be probability density functions, though, note that the unit integral constraint representation was chosen just for the sake of convenient interpretation. In [6], it is proven that $\mathcal{B}^2(I)$ endowed with the operations (\oplus, \odot) is a vector space. Note that the neutral elements of perturbation and powering are $e(x) = 1/\eta$, with $\eta = b - a$ (i.e., the uniform density), and 1, respectively. The difference between two elements $f, g \in \mathcal{B}^2(I)$, denoted by $f \ominus g$, is obtained as perturbation of f with the reciprocal of g , i.e., $(f \ominus g)(x) = (f \oplus [(-1) \odot g])(x)$, $x \in I$. Finally, to complete the Hilbert space structure, the inner product is defined as

$$\langle f, g \rangle_{\mathcal{B}} = \frac{1}{2\eta} \int_I \int_I \ln \frac{f(x)}{f(y)} \ln \frac{g(x)}{g(y)} dx dy, \quad f, g \in \mathcal{B}^2(I). \quad (2)$$

Form of the inner product clearly indicates that the relevant information in densities is contained in (log-)ratios between elements from the support I .

Density functions can be considered as functional counterparts to compositional data, positive vectors carrying relative information [1, 17] that are driven by the Aitchison geometry [16]. In order to enable their statistical processing using standard multivariate methods in real space [5], the preferred strategy is to express them either in centered log-ratio (clr) coefficients [1] with respect to a generating system, or in logratio coordinates, preferably with respect to an orthonormal basis [7]. The latter coordinates (called also isometric log-ratio coordinates), as well as the clr coefficients, provide isometry between the Aitchison geometry and the real Euclidean space. A similar strategy is used also for densities in the Bayes space [22]. An isometric isomorphism between $\mathcal{B}^2(I)$ and $L^2(I)$ is represented by the *centered log-ratio* (clr) transformation [14, 22], defined for $f \in \mathcal{B}^2(I)$ as

$$\text{clr}(f)(x) \equiv f_c(x) = \ln f(x) - \frac{1}{\eta} \int_I \ln f(y) dy. \quad (3)$$

We remark that such an isometry allows to compute operations and inner products among the elements in $\mathcal{B}^2(I)$ in terms of their counterpart in $L^2(I)$ among the clr-transforms, i.e.

$$\text{clr}(f \oplus g)(x) = f_c(x) + g_c(x), \quad \text{clr}(\alpha \odot f)(x) = \alpha \cdot f_c(x)$$

and

$$\langle f, g \rangle_{\mathcal{B}} = \langle f_c, g_c \rangle_2 = \int_I f_c(x) g_c(x) dx.$$

However, the clr transformation induces an additional constraint,

$$\int_I \text{clr}(f)(x) dx = \int_I \ln f(x) dx - \int_I \frac{1}{\eta} \int_I \ln f(y) dy dx = 0, \quad (4)$$

that needs to be taken into account for computation and analysis on clr-transformed density functions. As the clr space is clearly a subspace of $L^2(I)$, hereafter it is denoted as $L_0^2(I)$. The inverse clr transformation is obtained as

$$\text{clr}^{-1}[f_c](x) = \frac{\exp(f_c(x))}{\int_I \exp(f_c(y)) dy}; \quad (5)$$

again as before, the denominator is used just to achieve the unit integral constraint representation of the resulting density (without loss of relative information, carried by the density function).

According to [22], it is not necessary to restrict ourselves to the constrained clr space, because a basis in $\mathcal{B}^2(I)$ can be easily constructed. Specifically, let $\psi_0(x), \psi_1(x), \psi_2(x), \dots$ is a basis in $L^2(I)$ and assume that $\psi_0(x)$ is a constant function, then $\varphi_1(x) := \exp(\psi_1(x)), \varphi_2(x) := \exp(\psi_2(x)), \dots$ form a basis in $\mathcal{B}^2(I)$. Of course, also here an orthonormal basis is preferable, but it is not always possible in applications. Nevertheless, if this would be so, then a function $f \in \mathcal{B}^2(I)$ can be projected orthogonally to the space spanned, e.g., by the first r functions $\varphi_1(x), \varphi_2(x), \dots, \varphi_r(x)$. This is done through the respective coefficients c_1, \dots, c_r in the basis expansion

$$f(x) = c_1 \odot \varphi_1(x) \oplus c_2 \odot \varphi_2(x) \oplus \dots \oplus c_r \odot \varphi_r(x) \oplus \dots = \bigoplus_{i=1}^{\infty} c_i \odot \varphi_i(x), \quad x \in I. \quad (6)$$

Functional data analysis relies strongly on approximation of the input functions using splines [18]. However, splines are mostly utilized purely as an approximation tool, without considering further methodological consequences. Because statistical processing of density functions requires a deeper geometrical background, provided by the Bayes spaces, this should be followed also by the respective spline representation, performed preferably in the clr space $L_0^2(I)$. In [12], a first attempt of constructing a spline representation that would honor the zero integral constraint (4) was performed. The problem is that B -splines that form basis for the spline expansion in [12] come from $L^2(I)$, but not from $L_0^2(I)$. This paper presents an important step ahead – such splines are constructed that form basis functions in the clr space $L_0^2(I)$. Consequently, the splines can be expressed also directly in $\mathcal{B}^2(I)$ and the spline representation formulated in terms of the Bayes space which can be used for interpretation purposes; hereafter we refer to *compositional splines*. Apart from methodological advantages, using compositional splines simplifies construction and interpretation of spline coefficients that can be considered as coefficients of a (possibly orthonormal) basis in $\mathcal{B}^2(I)$.

The paper is organized as follows. In the next section the construction of splines basis in $L_0^2(I)$ is presented together with a comparison to spline functions introduced in [12]. Section 3 is devoted to smoothing splines in $L_0^2(I)$ and Section 4 discusses orthogonalization of basis functions (that form, by construction, an oblique basis). Section 5 introduces a new class of splines that reflect the Bayes spaces methodology, compositional splines. Section 6 demonstrates usefulness of the new approximation tool in context of simplicial functional principal component analysis with anthropometric data and the final Section 7 concludes.

2 Construction of spline in $L_0^2(I)$

Because the clr transformation enables to process density functions in the standard L^2 space, just restricted according to zero integral constraint (4), it is natural that also construction of compositional splines should start in $L_0^2(I)$. Nevertheless, before doing so, some basic facts about B -spline representation of splines are recalled, see [2, 4, ?] for details. Let the sequence of knots

$$\lambda_0 = a < \lambda_1 < \dots < \lambda_g < b = \lambda_{g+1}$$

be given. The (normalized) B -spline of degree 0 (order 1) is defined as

$$B_i^1(x) = \begin{cases} 1 & \text{if } x \in [\lambda_i, \lambda_{i+1}) \\ 0 & \text{otherwise} \end{cases}$$

and the (normalized) B -spline of degree k , $k \in \mathbb{N}$, (order $k + 1$) is defined by

$$B_i^{k+1}(x) = \frac{x - \lambda_i}{\lambda_{i+k} - \lambda_i} B_i^k(x) + \frac{\lambda_{i+k+1} - x}{\lambda_{i+k+1} - \lambda_{i+1}} B_{i+1}^k(x).$$

Now let the functions $Z_i^{k+1}(x)$ for $k \geq 0$, $k \in \mathbb{N}$, be defined

$$Z_i^{k+1}(x) := \frac{d}{dx} B_i^{k+2}(x), \tag{7}$$

i.e., more precisely for $k = 0$

$$Z_i^1(x) = \begin{cases} \frac{1}{\lambda_{i+1} - \lambda_i} & \text{if } x \in [\lambda_i, \lambda_{i+1}) \\ \frac{-1}{\lambda_{i+2} - \lambda_{i+1}} & \text{if } x \in (\lambda_{i+1}, \lambda_{i+2}] \end{cases}$$

and for $k \geq 1$

$$Z_i^{k+1}(x) = (k+1) \left(\frac{B_i^{k+1}(x)}{\lambda_{i+k+1} - \lambda_i} - \frac{B_{i+1}^{k+1}(x)}{\lambda_{i+k+2} - \lambda_{i+1}} \right). \quad (8)$$

Noteworthy, functions $Z_i^{k+1}(x)$ have similar properties as B -splines $B_i^{k+1}(x)$.

1. They are piecewise polynomials of degree k . Particularly, $Z_i^1(x)$ is a piecewise constant polynomial, $Z_i^2(x)$ is a piecewise linear polynomial, see Figure 1, $Z_i^3(x)$ is a piecewise quadratic polynomial, see Figure 2. For other examples see Figures 3-5.
2. It is evident that for $k \geq 1$ the function $Z_i^{k+1}(x)$ and its derivatives up to order $k-1$ are all continuous.
3. It is easy to check that for $k \geq 0$

$$\text{supp } Z_i^{k+1}(x) = \text{supp } B_i^{k+2}(x) = [\lambda_i, \lambda_{i+k+2}],$$

and of course

$$Z_i^{k+1}(x) = 0 \quad \text{if } x \notin [\lambda_i, \lambda_{i+k+2}].$$

4. From the perspective of $L_0^2(I)$, a crucial point is that the integral of $Z_i^{k+1}(x)$ equals to zero. If we consider Curry-Schoenberg B -spline $M_i^{k+1}(x)$ [2], which are defined as

$$M_i^{k+1}(x) := \frac{k+1}{\lambda_{i+k+1} - \lambda_i} B_i^{k+1}(x)$$

with property

$$\int_{\mathbb{R}} M_i^{k+1}(x) dx = 1,$$

than it is clear that

$$Z_i^{k+1}(x) = M_i^{k+1}(x) - M_{i+1}^{k+1}(x) \quad (9)$$

and

$$\int_{\mathbb{R}} Z_i^{k+1}(x) dx = 0.$$

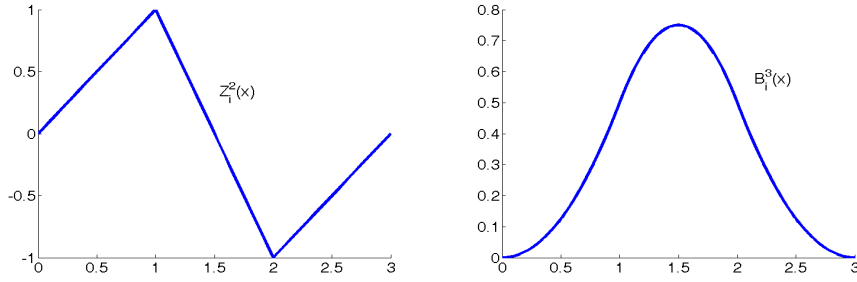


Figure 1: The piecewise linear function $Z_i^2(x) = \frac{d}{dx}B_i^3(x)$ with equidistant knots 0, 1, 2, 3.

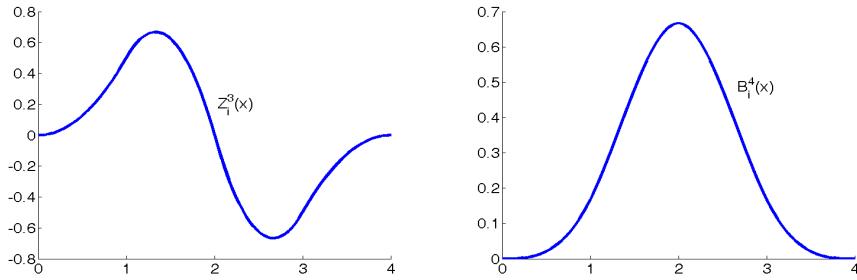


Figure 2: The piecewise quadratic function $Z_i^3(x) = \frac{d}{dx}B_i^4(x)$ with equidistant knots 0, 1, 2, 3, 4.

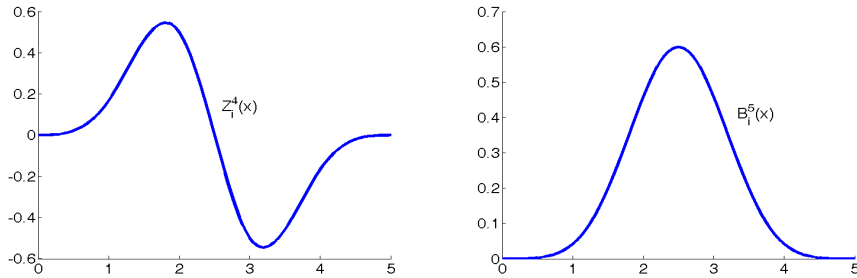


Figure 3: The piecewise cubic function $Z_i^4(x) = \frac{d}{dx}B_i^5(x)$ with equidistant knots 0, 1, 2, 3, 4, 5.

It is known that for the vector space $\mathcal{S}_k^{\Delta\lambda}[a, b]$ of polynomial splines of degree $k > 0$, $k \in \mathbb{N}$, defined on a finite interval $I = [a, b]$ with the sequence of knots $\Delta\lambda = \{\lambda_i\}_{i=0}^{g+1}$, $\lambda_0 = a < \lambda_1 < \dots < \lambda_g < b = \lambda_{g+1}$, the dimension is

$$\dim(\mathcal{S}_k^{\Delta\lambda}[a, b]) = g + k + 1.$$

For the construction of all basis functions $B_i^{k+1}(x)$, it is necessary to consider some addi-

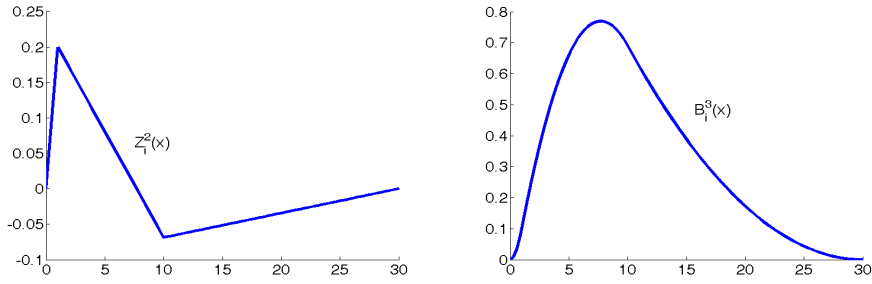


Figure 4: The piecewise linear function $Z_i^2(x) = \frac{d}{dx}B_i^3(x)$ with nonequidistant knots $0, 1, 10, 30$.

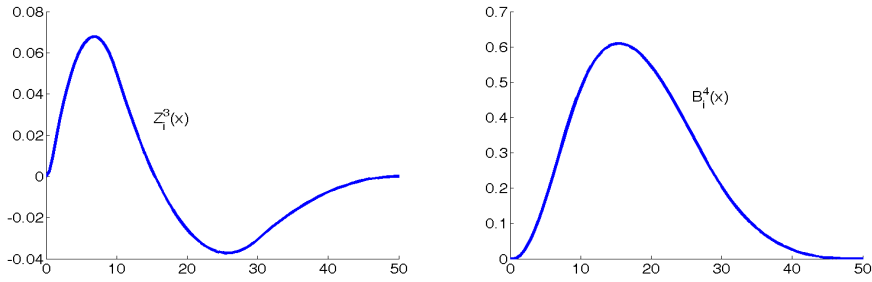


Figure 5: The piecewise quadratic function $Z_i^3(x) = \frac{d}{dx}B_i^4(x)$ with nonequidistant knots $0, 1, 10, 30, 50$.

tional knots. Without loss of generality we can add coincident knots

$$\lambda_{-k} = \dots = \lambda_{-1} = \lambda_0 = a, \quad b = \lambda_{g+1} = \lambda_{g+2} = \dots = \lambda_{g+k+1}. \quad (10)$$

Then every spline $s_k(x) \in \mathcal{S}_k^{\Delta\lambda}[a, b]$ in $L^2(I)$ has a unique representation

$$s_k(x) = \sum_{i=-k}^g b_i B_i^{k+1}(x). \quad (11)$$

In [12, 20], the splines with zero integral are studied. There is given the necessary and sufficient condition for B -splines coefficients of these splines. However, typical B -splines $B_i^{k+1}(x)$, thus ignoring the constraint (4) in $L_0^2(I)$ for construction of the B -spline basis, were used there.

Now, regarding the definition (7), we are able to use spline functions $Z_i^{k+1}(x)$ which have zero integral on I (denoted also as ZB -splines in the sequel). In the following, $\mathcal{Z}_k^{\Delta\lambda}[a, b]$ denotes the vector space of polynomial splines of degree $k > 0$, defined on a finite interval $[a, b]$ with the sequence of knots $\Delta\lambda$ and having zero integral on $[a, b]$, it means

$$\mathcal{Z}_k^{\Delta\lambda}[a, b] := \{s_k(x) \in \mathcal{S}_k^{\Delta\lambda}[a, b] : \int_I s_k(x) dx = 0\}. \quad (12)$$

Theorem 2.1. *The dimension of the vector space $\mathcal{Z}_k^{\Delta\lambda}[a, b]$ defined by the formula (12) is $g + k$.*

Proof. For spline $s_k(x) \in \mathcal{S}_k^{\Delta\lambda}[a, b]$, $s_k(x) = \sum_{i=-k}^g b_i B_i^{k+1}(x)$, with the coincident additional knots it is known, [4], that

$$\int_I s_k(x) dx = \frac{1}{k+1} \sum_{i=-k}^g b_i (\lambda_{i+k+1} - \lambda_i).$$

It means that B -spline coefficients of $s_k(x) \in \mathcal{Z}_k^{\Delta\lambda}[a, b] \subset \mathcal{S}_k^{\Delta\lambda}[a, b]$ satisfy condition $0 = \sum_{i=-k}^g b_i (\lambda_{i+k+1} - \lambda_i) = \mathbf{A}\mathbf{b}$ with $\mathbf{A} = (\lambda_1 - \lambda_{-k}, \dots, \lambda_{g+k+1} - \lambda_g)$, $\mathbf{b} = (b_{-k}, \dots, b_g)^\top$. And it is obvious that $\text{codim}(\mathcal{Z}_k^{\Delta\lambda}[a, b]) = 1$, thus

$$\dim(\mathcal{Z}_k^{\Delta\lambda}[a, b]) = \dim(\mathcal{S}_k^{\Delta\lambda}[a, b]) - \text{codim}(\mathcal{Z}_k^{\Delta\lambda}[a, b]) = g + k.$$

□

Theorem 2.2. *For the coincident additional knots (10), the functions $Z_{-k}^{k+1}(x), \dots, Z_{g-1}^{k+1}(x)$ form a basis for the space $\mathcal{Z}_k^{\Delta\lambda}[a, b]$.*

Proof. Since $M_i^{k+1}(x)$ form a basis for the spline space $\mathcal{S}_k^{\Delta\lambda}[a, b]$ and $Z_i^{k+1}(x) = M_i^{k+1}(x) - M_{i+1}^{k+1}(x)$, the functions $Z_i^{k+1}(x)$, $i = -k, \dots, g-1$, are linearly independent and lie in $\mathcal{Z}_k^{\Delta\lambda}[a, b]$ with $\dim(\mathcal{Z}_k^{\Delta\lambda}[a, b]) = g + k$. Therefore $Z_i^{k+1}(x)$, $i = -k, \dots, g-1$, form a basis for the $\mathcal{Z}_k^{\Delta\lambda}[a, b]$. □

With regard to this theorem, every spline $s_k(x) \in \mathcal{Z}_k^{\Delta\lambda}[a, b]$ has a unique representation

$$s_k(x) = \sum_{i=-k}^{g-1} z_i Z_i^{k+1}(x). \quad (13)$$

Now we can proceed to matrix notation of $s_k(x) \in \mathcal{Z}_k^{\Delta\lambda}[a, b]$. With respect to (8) and (9), we are able to write the functions $Z_i^{k+1}(x)$ in matrix notation as

$$Z_i^{k+1}(x) = (k+1) (B_i^{k+1}(x), B_{i+1}^{k+1}(x)) \begin{pmatrix} \frac{1}{\lambda_{i+k+1} - \lambda_i} & 0 \\ 0 & \frac{1}{\lambda_{i+k+2} - \lambda_{i+1}} \end{pmatrix} \begin{pmatrix} 1 \\ -1 \end{pmatrix}.$$

Then it is clear that

$$(Z_{-k}^{k+1}(x), \dots, Z_{g-1}^{k+1}(x)) = (B_{-k}^{k+1}(x), \dots, B_g^{k+1}(x)) \mathbf{DK} = \mathbf{B}_{k+1}(x) \mathbf{DK},$$

where

$$\mathbf{D} = (k+1) \text{diag} \left(\frac{1}{\lambda_1 - \lambda_{-k}}, \dots, \frac{1}{\lambda_{g+k+1} - \lambda_g} \right) = (k+1) \text{diag} \left(\frac{1}{l_1}, \dots, \frac{1}{l_{g+k+1}} \right) \quad (14)$$

and

$$\mathbf{K} = \begin{pmatrix} 1 & 0 & 0 & \cdots & 0 & 0 \\ -1 & 1 & 0 & \cdots & 0 & 0 \\ 0 & -1 & 1 & \cdots & 0 & 0 \\ \vdots & \vdots & \ddots & \ddots & \vdots & \vdots \\ 0 & 0 & 0 & \cdots & -1 & 1 \\ 0 & 0 & 0 & \cdots & 0 & -1 \end{pmatrix} \in \mathbb{R}^{g+k+1, g+k}. \quad (15)$$

Therefore the spline $s_k(x) \in \mathcal{Z}_k^{\Delta\lambda}[a, b]$, $s_k(x) = \sum_{i=-k}^{g-1} b_i Z_i^{k+1}(x)$ can be written in matrix notation as

$$s_k(x) = \mathbf{Z}_{k+1}(x)\mathbf{z} = \mathbf{B}_{k+1}(x)\mathbf{D}\mathbf{K}\mathbf{z}, \quad (16)$$

where $\mathbf{Z}_{k+1}(x) = (Z_{-k}^{k+1}(x), \dots, Z_{g-1}^{k+1}(x))$ and $\mathbf{z} = (z_{-k}, \dots, z_{g-1})^\top$.

Remark 1. *The formula (16) is very useful, because we can use the standard B-spline basis for working with splines honoring the zero integral constraint, which is very convenient from a computational point of view.*

Example 2.1. *We consider knots $\Delta\lambda = \{\lambda_i\}_{i=0}^{g+1}$, $\lambda_0 = 0 = a < 2 < 5 < 9 < 14 < b = 20 = \lambda_5$. The task is to find a cubic spline with the given sequence of knots and which has zero integral on the interval $[0, 20]$. It is evident that $k = 3$, $g = 4$. We consider the additional knots*

$$\lambda_{-3} = \lambda_{-2} = \lambda_{-1} = \lambda_0 = a = 0, \quad 20 = b = \lambda_5 = \lambda_6 = \lambda_7 = \lambda_8.$$

The basis functions of the space $\mathcal{Z}_3^{\Delta\lambda}[0, 20]$ are plotted in Figure 7. Every spline $s_3(x) \in \mathcal{Z}_3^{\Delta\lambda}[0, 20]$ can be written as

$$s_3(x) = \sum_{i=-3}^3 z_i Z_i^4(x). \quad (17)$$

Thus, e.g., for $\mathbf{z} = (z_{-3}, \dots, z_3)^\top = (0.5, -1, 2, 3, -8, 9, 1)^\top$ the cubic spline $s_3(x)$ with zero integral is plotted in Figure 6.

3 Smoothing spline in $L_0^2(I)$

In [12], the construction of smoothing splines in the space $L_0^2(I)$ was studied, however using standard B-spline basis functions $B_i^{k+1}(x)$. Now we are able to construct smoothing splines in this space with new basis functions $Z_i^{k+1}(x)$. For this purpose, let data (x_i, y_i) , $a \leq x_i \leq b$, weights $w_i > 0$, $i = 1, \dots, n$, sequence of knots $\Delta\lambda = \{\lambda_i\}_{i=0}^{g+1}$, $\lambda_0 = a < \lambda_1 < \dots < \lambda_g < b = \lambda_{g+1}$, $n \geq g + 1$ and a parameter $\alpha \in (0, 1)$ be given. For arbitrary $l \in \{1, \dots, k - 1\}$ our task is to find a spline $s_k(x) \in \mathcal{Z}_k^{\Delta\lambda}[a, b] \subset L_0^2(I)$, which minimizes the functional

$$J_l(s_k) = (1 - \alpha) \int_a^b [s_k^{(l)}(x)]^2 dx + \alpha \sum_{i=1}^n w_i [y_i - s_k(x_i)]^2.$$

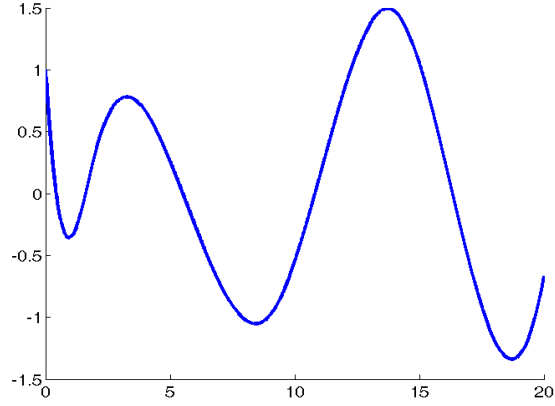


Figure 6: Cubic spline $s_3(x)$ with given coefficients $\mathbf{z} = (0.5, -1, 2, 3, -8, 9, 1)^\top$.

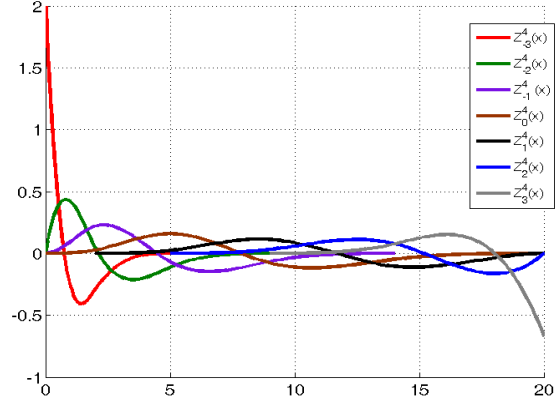


Figure 7: Basis splines for the space $\mathcal{Z}_3^{\Delta\lambda}[0, 20]$.

Note that the choice of parameter α and l , where l stands for l th derivation, affects smoothness of the resulting spline. Let us denote $\mathbf{x} = (x_1, \dots, x_n)^\top$, $\mathbf{y} = (y_1, \dots, y_n)^\top$, $\mathbf{w} = (w_1, \dots, w_n)^\top$ and $\mathbf{W} = \text{diag}(\mathbf{w})$. Regarding the representation (13) and matrix notation (16), the functional $J_l(s_k)$ can be written as a quadratic function

$$J_l(\mathbf{z}) = (1 - \alpha)\mathbf{z}^\top \mathbf{K}^\top \mathbf{D} \mathbf{S}_l^\top \mathbf{M}_{kl} \mathbf{S}_l \mathbf{D} \mathbf{K} \mathbf{z} + \alpha [\mathbf{y} - \mathbf{B}_{k+1}(\mathbf{x}) \mathbf{D} \mathbf{K} \mathbf{z}]^\top \mathbf{W} [\mathbf{y} - \mathbf{B}_{k+1}(\mathbf{x}) \mathbf{D} \mathbf{K} \mathbf{z}], \quad (18)$$

see [10, 11, 12] for details. In fact the matrix

$$\mathbf{M}_{kl} = (m_{ij}^{kl})_{i,j=-k+l}^g, \quad \text{with} \quad m_{ij}^{kl} = \int_a^b B_i^{k+1-l}(x) B_j^{k+1-l}(x) dx \quad (19)$$

is positive definite, because $B_i^{k+1-l}(x) \geq 0$, $i = -k + l, \dots, g$ are basis functions. Upper triangular matrix $\mathbf{S}_l = \mathbf{D}_l \mathbf{L}_l \dots \mathbf{D}_1 \mathbf{L}_1 \in \mathbb{R}^{g+k+1-l, g+k+1}$ has full row rank. $\mathbf{D}_j \in \mathbb{R}^{g+k+1-j, g+k+1-j}$ is a diagonal matrix such that

$$\mathbf{D}_j = (k+1-j) \text{diag}(d_{-k+j}, \dots, d_g)$$

with

$$d_i = \frac{1}{\lambda_{i+k+1-j} - \lambda_i}, \quad i = -k+j, \dots, g,$$

and

$$\mathbf{L}_j := \begin{pmatrix} -1 & 1 & & \\ & \ddots & \ddots & \\ & & -1 & 1 \end{pmatrix} \in \mathbb{R}^{g+k+1-j, g+k+2-j}.$$

Finally, $\mathbf{B}_{k+1}(\mathbf{x}) \in \mathbb{R}^{n, g+k+1}$ stands for the collocation matrix, i.e.

$$\mathbf{B}_{k+1}(\mathbf{x}) = (B_i^{k+1}(x_j))_{j=1, i=-k}^{n, g}.$$

Using the notation $\mathbf{U} := \mathbf{DK}$,

$$\mathbf{G} := \mathbf{U}^\top [(1-\alpha)\mathbf{S}_l^\top \mathbf{M}_{kl} \mathbf{S}_l + \alpha \mathbf{B}_{k+1}^\top(\mathbf{x}) \mathbf{W} \mathbf{B}_{k+1}(\mathbf{x})] \mathbf{U} \quad (20)$$

and

$$\mathbf{g} := \alpha \mathbf{K}^\top \mathbf{D} \mathbf{B}_{k+1}^\top(\mathbf{x}) \mathbf{W} \mathbf{y},$$

it is possible to rewrite the quadratic function $J_l(\mathbf{z})$ as

$$J_l(\mathbf{z}) = \mathbf{z}^\top \mathbf{G} \mathbf{z} - 2\mathbf{z}^\top \mathbf{g} + \alpha \mathbf{y}^\top \mathbf{W} \mathbf{y}. \quad (21)$$

Our task is to find a spline $s_k(x) \in \mathcal{Z}_k^{\Delta\lambda}[a, b]$ which minimizes the functional $J_l(s_k)$, in other words, we want to find a minimum of the function (21). It is obvious that this function has just one minimum if and only if the matrix \mathbf{G} is positive definite (p.d.). From (20) it can be easily seen that

$$\mathbf{G} \text{ is p.d.} \quad \Leftrightarrow \quad \mathbf{B}_{k+1}(\mathbf{x}) \text{ is of full column rank.}$$

From Schoenberg-Whitney theorem and its generalization, see [2] and [10], it is known that matrix $\mathbf{B}_{k+1}(\mathbf{x})$ is of full column rank if and only if there exists $\{u_{-k}, \dots, u_g\} \subset \{x_1, \dots, x_n\}$ with $u_i < u_{i+1}$, $i = -k, \dots, g-1$, such that $\lambda_i < u_i < \lambda_{i+k+1}$, $i = -k, \dots, g$. In this case from the necessary and sufficient condition for a unique minimum of quadratic function, i.e.

$$\frac{\partial J_l(\mathbf{z})}{\partial \mathbf{z}^\top} = 0,$$

we get a system of linear equations $\mathbf{G} \mathbf{z} = \mathbf{g}$ and then the unique solution of this system is given by

$$\mathbf{z}^* = \mathbf{G}^{-1} \mathbf{g}. \quad (22)$$

Consequently, the resulting smoothing spline is obtained by the formula

$$s_k^*(x) = \sum_{i=-k}^{g-1} z_i^* Z_i^{k+1}(x),$$

in matrix notation using standard B -splines $B_i^{k+1}(x)$ as

$$s_k^*(x) = \mathbf{B}_{k+1}(t) \mathbf{D} \mathbf{K} \mathbf{z}^*,$$

where the vector $\mathbf{z}^* = (z_{-k}^*, \dots, z_{g-1}^*)'$ is obtained as

.

4 Orthogonalization of basis functions

A further step is to orthogonalize the basis

$$\mathbf{Z}_{k+1}(x) = (Z_{-k}^{k+1}(x), \dots, Z_{g-1}^{k+1}(x))^\top$$

of the space $\mathcal{Z}_k^{\Delta\lambda}[a, b]$ that is by construction oblique with respect to the L^2 space metric. For this purpose the idea presented in [19] is used. We search for a linear transformation Φ such that

$$\mathbf{O}_{k+1}(x) = \Phi \mathbf{Z}_{k+1}(x)$$

forms an orthogonal set of basis functions of the space $\mathcal{Z}_k^{\Delta\lambda}[a, b]$, i.e.

$$\int_a^b \mathbf{O}_{k+1}(x) \mathbf{O}_{k+1}^\top(x) dx = \mathbf{I}.$$

Regarding the lemma presented in [19] and notation used here, we can formulate the following statement.

Lemma 4.1. *An invertible transformation Φ orthogonalizes the basis functions $\mathbf{Z}_{k+1}(x)$ if and only if it satisfies the condition that*

$$\Phi^\top \Phi = \Sigma^{-1},$$

where Σ represents the positive definite matrix

$$\Sigma = \int_a^b \mathbf{Z}_{k+1}(x) \mathbf{Z}_{k+1}^\top(x) dx = \left(\int_a^b Z_i^{k+1}(x) Z_j^{k+1}(x) dx \right)_{i,j=-k}^{g-1}.$$

With respect to the definition of basis functions $\mathbf{Z}_{k+1}(x) = (Z_{-k}^{k+1}(x), \dots, Z_{g-1}^{k+1}(x))^\top$ the matrix Σ can be expressed as

$$\Sigma = \mathbf{K}^\top \mathbf{D} \mathbf{M} \mathbf{D} \mathbf{K}, \tag{23}$$

where $\mathbf{M} := \mathbf{M}_{k0}$. The linear transformation Φ is not unique and can be computed for example by the Cholesky decomposition. The basis functions

$$\mathbf{O}_{k+1}(x) = \Phi \mathbf{Z}_{k+1}(x), \quad \mathbf{O}_{k+1}(x) = (O_{-k}^{k+1}(x), \dots, O_{g-1}^{k+1}(x))^\top$$

are orthogonal and have a zero integral. The linear and quadratic ZB -splines with zero integral and their orthogonalization are plotted in Figures 8 and 9.

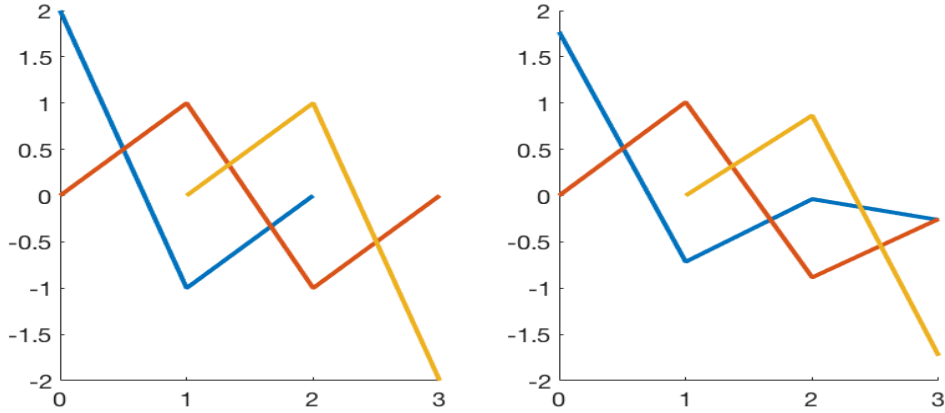


Figure 8: Linear ZB -splines $Z_i^2(x)$ with given knots 0, 0, 1, 2, 3, 3 (left), linear orthogonal ZB -splines $O_i^2(x)$ (right).

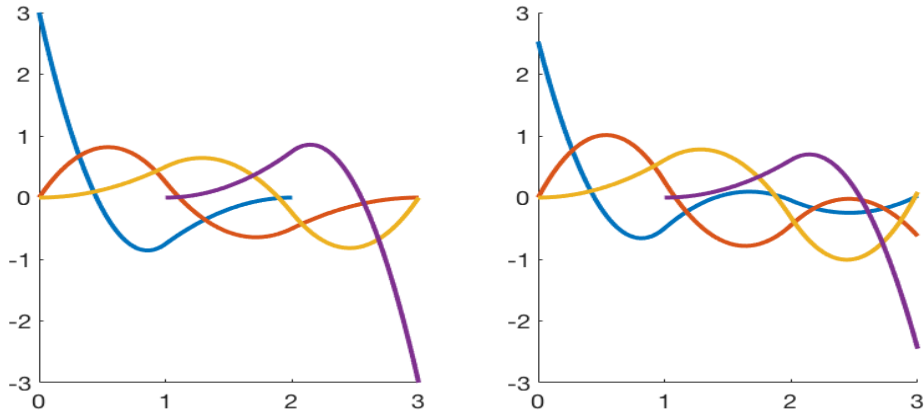


Figure 9: Quadratic ZB -splines $Z_i^3(x)$ with given knots 0, 0, 0, 1, 2, 3, 4, 4, 4 (left), quadratic orthogonal ZB -splines $O_i^3(x)$ (right).

To sum up, the spline $s_k(x)$ with zero integral can be constructed as a linear combination of orthogonal splines $O_i^{k+1}(x)$ having zero integral in a form

$$s_k(x) = \sum_{i=-k}^{g-1} z_i O_i^{k+1}(x) = \mathbf{O}_{k+1}(x) \mathbf{z}.$$

On the other hand, the standard and well-known B -splines $B_i^{k+1}(x)$ can be used to represent $s_k(x) \in \mathcal{Z}_k^{\Delta\lambda}[a, b]$ in matrix form

$$s_k(x) = \Phi \mathbf{B}_{k+1}(x) \mathbf{D} \mathbf{K} \mathbf{z}.$$

This formulation seems to be very useful because it allows us to use existing B -spline codes in software R or Matlab, for example, the collocation matrix or computation of integrals in (19).

5 Compositional splines in the Bayes space

Construction of splines directly in $L_0^2(I)$ has important practical consequences, however, it is crucial also from the theoretical perspective. Expressing splines as functions in $L_0^2(I)$ enables to back-transform them to the original Bayes space $\mathcal{B}^2(I)$ using (5). It results in *compositional CB-splines*, obtained from (8) as

$$\zeta_i^{k+1}(x) = \frac{\exp[Z_i^{k+1}(x)]}{\int_I \exp[Z_i^{k+1}(y)] dy}, \quad i = -k, \dots, g-1, \quad k \geq 0. \quad (24)$$

Accordingly, for instance ZB -splines from Figures 1-5 can be now expressed directly in the Bayes space $\mathcal{B}^2(I)$ as CB -splines, see Figures 10-12. Note that CB -splines $\zeta_i^{k+1}(x)$ fulfill the unit integral constraint which is, however, not necessary for further considerations. As a consequence, it is immediate to define vector space $\mathcal{C}_k^{\Delta\lambda}[a, b]$ of compositional polynomial splines of degree $k > 0$, defined on a finite interval $[a, b]$ with the sequence of knots $\Delta\lambda$. From isomorphism between $\mathcal{C}_k^{\Delta\lambda}[a, b]$ and $\mathcal{Z}_k^{\Delta\lambda}[a, b]$ it holds that

$$\dim(\mathcal{C}_k^{\Delta\lambda}[a, b]) = g + k.$$

Moreover, from isometric properties of clr transformation it follows that every compositional spline $\xi_k(x) \in \mathcal{C}_k^{\Delta\lambda}[a, b]$ in $\mathcal{B}^2(I)$ can be uniquely represented as

$$\xi_k(x) = \bigoplus_{i=-k}^{g-1} z_i \odot \zeta_i^{k+1}(x). \quad (25)$$

CB -splines $\zeta_i^{k+1}(x)$ forming the basis are by the default setting (8) not orthogonal. Their orthogonalization can be done as described in Section 4, i.e. by employing $L_0^2(I)$ with the back-transformation to $\mathcal{B}^2(I)$.

The resulting compositional splines (with either orthogonal, or non-orthogonal CB -spline basis) can be used for representation of densities directly in $\mathcal{B}^2(I)$. This is an important step in construction of methods of functional data analysis involving density functions, like for ANOVA modeling [22] or for the SFPCA method introduced in [9] and demonstrated in the next section. In the latter case CB -splines were indeed already used for construction of the procedure, although at the respective level of development the authors were not aware of that. With CB -splines one has a guarantee that methods are developed consistently

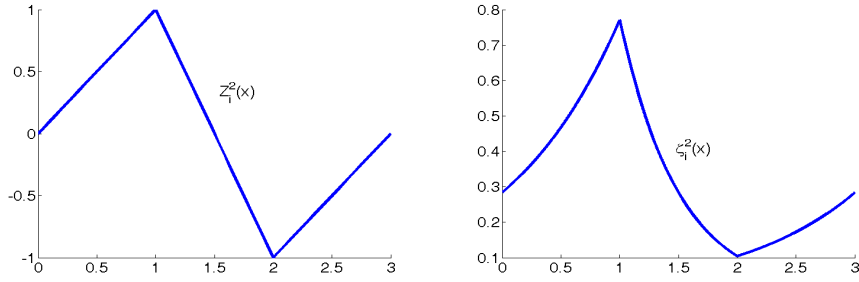


Figure 10: Linear ZB -spline $Z_i^2(x)$ (left) and linear CB -spline $\zeta_i^2(x)$ (right) with equidistant knots 0, 1, 2, 3.

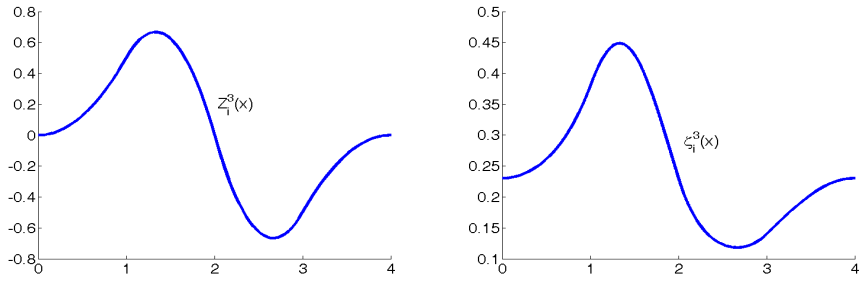


Figure 11: Quadratic ZB -spline $Z_i^3(x)$ (left) and quadratic CB -spline $\zeta_i^3(x)$ (right) with equidistant knots 0, 1, 2, 3, 4.

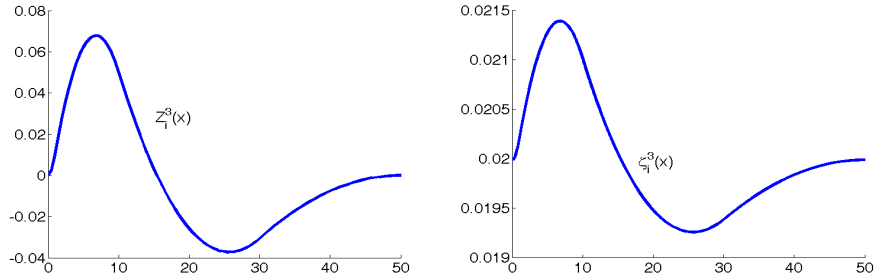


Figure 12: Quadratic ZB -spline $Z_i^3(x)$ (left) and quadratic CB -spline $\zeta_i^3(x)$ (right) with nonequidistant knots 0, 1, 10, 30, 50.

in the Bayes space. Moreover, the possibility of having an orthogonal basis enables to gain additional features resulting from orthogonality of finite dimensional projection in combination with approximate properties of spline functions.

As usual, compositional splines can be tuned according to concrete problem, with the advantage of their direct formulation in the Bayes space sense.

Example 5.1. *To illustrate smoothing of concrete data with a compositional spline, 1000*

values from standard normal distribution were simulated and the support was determined by minimum and maximum simulated values, $I = [x_{min}, x_{max}]$. Data were collected in a form of histogram, where the breakpoints are equidistantly spaced. The representative points of the histogram cells are denoted as asterisks in Figure 13 (left) and these points form the input data (x_i, y_i) , $i = 1, \dots, n$ for smoothing purpose. The y -values stand for discretized relative contributions to the overall probability mass, therefore discrete clr transformation [1] is needed to obtain a real vector with zero sum constraint (Figure 13, right). These data points were smoothed using the procedure from Section 3 and back-transformed to the original space. In the concrete setting $k = 2$, $l = 1$, $\alpha = 0.5$, $\Delta\lambda = \{x_1, -2, -1, 0, 1, 2, x_n\}$, $w_i = 1$, $\forall i = 1, \dots, n$ were considered. The resulting spline $s_2(x)$ with zero integral on interval $[x_{min}, x_{max}]$ is plotted in Figure 13 (right). In the left plot the compositional spline $\xi_2(x)$ with unit integral by using (5) is depicted.

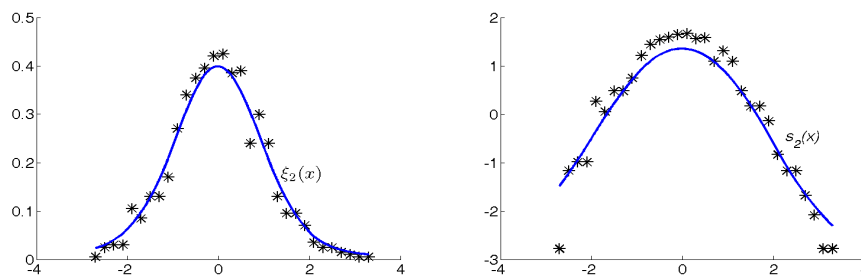


Figure 13: Smoothing of simulated standard normal values in the Bayes space (left) and for clr transformed data (right).

6 Application to anthropometric data

For the purpose of illustrating the smoothing procedure outlined in Section 3, a real-world data set dealing with the most commonly used anthropometric measure relating to body weight is presented. The data set we consider collects the body weight of apparently healthy Czech adolescents and young adults aged 15-31 years (the total of 4436 records) which were recruited non-randomly by offering free body composition assessment. Body weight was measured by the InBody 720 device (Biospace Co., Ltd, Seoul, Korea), recorded as the total body mass rounded to the nearest 0.1 kg.

The raw data for each of $N = 16$ age groups, i.e. $[15, 16)$, $[16, 17)$, \dots , $[30, 31)$, were turned into a form of histogram data as follows. The sampled values of the body weight in each age group were divided into equally-spaced classes of the united range 40-110 kg and the optimal number of classes, denoted by q_i , $i = 1, \dots, 16$, was set according to the well-known Sturge's rule separately across the age groups. Because of the insufficient number of sampled data for males and females in each age group, gender information was ignored. Although there might be some differences between male and female samples due to sex dimorphism, they are not that dramatic (e.g., contrary to body height) because the

weight is influenced also by external factors (nutrition, physical activity), and still allow for a reasonable aggregation of data. Subsequently, the proportions in classes within each age group were computed and present zero-values (zero counts in the respective classes) were imputed by values $(2/3) \cdot (1/n_i), i = 1, \dots, N$ according to [13], where n_i stands for the number of observations in i th age group. Finally, the raw discretized density data $f_{i,j}, i = 1, \dots, N, j = 1, \dots, q_i$ which correspond to the midpoints $t_{i,j}$ of classes, $i = 1, \dots, N, j = 1, \dots, q_i$ (i.e., $f_{i,j} = f(t_{i,j})$), were obtained by dividing (not necessary normalized) proportions $\mathbf{p}_i = (p_{i,1}, \dots, p_{i,q_i})^\top$ of counts in classes by the length of the respective intervals resulting from partition of the weight range in each of age groups. Figure 14 shows four examples of histograms with different number of classes together with raw data (Table 1) to be smoothed. To do so, their transformation into real vectors is needed. We note that if the histogram data are constructed on subintervals of the same length, i.e. with equally-spaced breakpoints, it enables to use the discrete version of the clr transformation [1] directly on the vector of proportions $\mathbf{p}_i, i = 1, \dots, N$ by considering the scale invariance property. Otherwise, the input of the clr transformation must be vectors with raw density data $\mathbf{f}_i = (f_{i,1}, \dots, f_{i,q_i})^\top, i = 1, \dots, N$ in order to avoid misleading results which would not reflect the actual behavior of data. Vectors of clr transforms are hereafter denoted as $\text{clr}(\mathbf{f}_i) = (\text{clr}(f_{i,1}), \dots, \text{clr}(f_{i,q_i}))^\top$ for $i = 1, \dots, N$ and clr values are listed in Table 2.

Having the collected data $(t_{i,j}, \text{clr}(f_{i,j}))$, we proceed to smooth them with the compositional smoothing splines using a system of ZB -spline basis functions from the $L_0^2(I)$. They are considered on domain $I = [40, 107]$ which has been modified in order to avoid undesired artifacts in densities at their right-hand side. For all N observations, the same strategy was followed to set the values of the input parameters for the smoothing procedure. We employed cubic smoothing splines ($k = 3, l = 2$) with the given sequence of knots $\Delta\lambda = \{40, 62, 84, 107\}$, the vectors of weights \mathbf{w}_i for all input data equal to vectors of ones and the smoothing parameter α was set to 0.5. That is, when minimizing the penalized functional (18), the same importance is assigned to both smoothness of the smoothing splines as well as to their approximative properties. The resulting compositional smoothing splines are obtained via their clr representation

$$s_3^i(t) = \sum_{\nu=-3}^1 z_{i,\nu} Z_\nu^4(t), \quad i = 1, \dots, N, \quad t \in I; \quad (26)$$

the corresponding ZB -spline coefficients are reported in Table 3.

Figure 15a displays an example of three raw density data from Figure 14 together with smoothed curves in the L_0^2 space (right) and after the inverse transformation (5) in the \mathcal{B}^2 space (left). The whole sample of smoothed density functions (Figure 15b) is plotted on blue scale distinguishing the age groups. Two trends are apparent – in the younger age groups, the estimated density functions are right skewed and exhibit lower variability while with increasing age they become more symmetric followed by higher variability. Nevertheless, density function in age group [23, 24] does not fully respect this behavior: the variability trend holds, but the distribution of weights is more similar to those in younger age groups as it is skewed more to the left. In general, it seems that adolescents

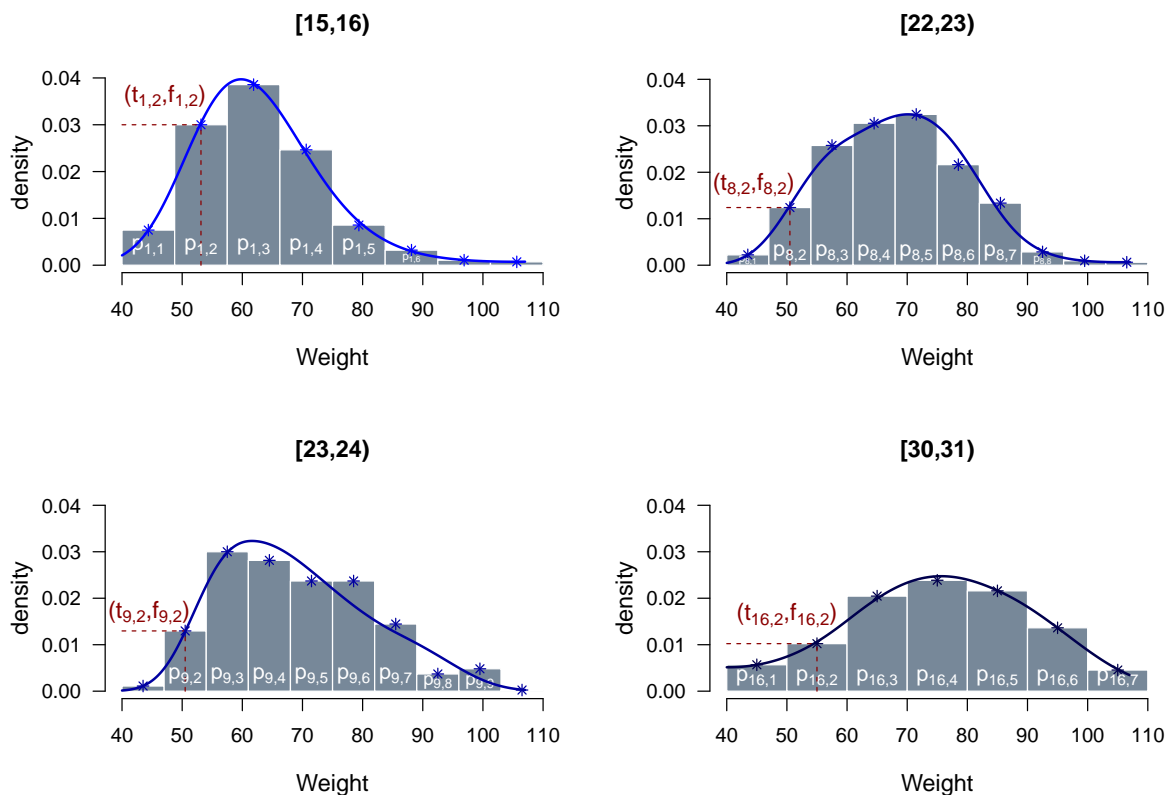
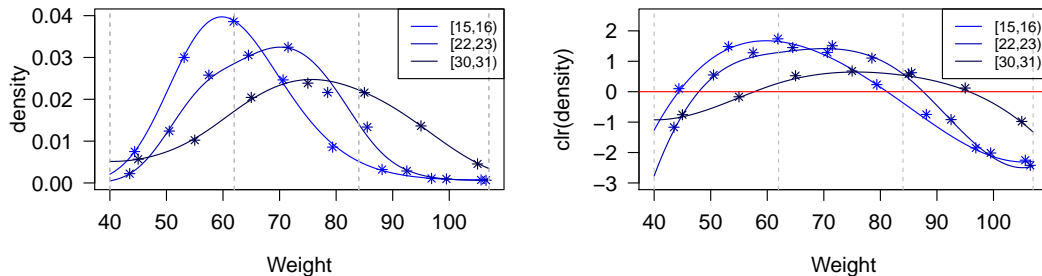


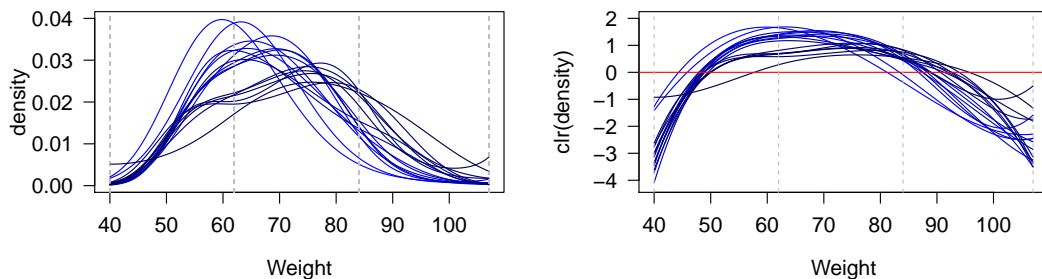
Figure 14: Histograms for four age groups: $[15, 16)$, $[22, 23)$, $[23, 24)$ and $[30, 31)$ together with estimated probability density functions via compositional smoothing splines. Asterisks indicate discrete data $(t_{i,j}, f_{i,j})$, $i = 1, 8, 9, 16$, $j = 1, 2, \dots, q_i$, and p_{ij} , $i = 1, 8, 9, 16$, $j = 1, 2, \dots, q_i$ indicate proportions of equidistant classes resulted for given partition of the range weight body values.

appear to be predominantly of a lower body weight than the older persons whose weight is more spread over the weight classes and more pronounced in the middle part of the distribution. Accordingly, there is also a higher incidence of higher weights in comparison with the younger adolescents.

Importantly, the quality of smoothing is the same irrespective of the shape of the distribution. It might just happen that the smoothed densities exhibit heavier tails although they are not indicated by the data $f_{i,j}$, even with some artifacts typical for overfitting. This is obviously due to keeping the zero integral constraint, which is more sensitive to deviations from monotonic character of densities at their tails. A possible way out, applied here, was to reduce slightly the range from $I = [40, 110]$ to $I = [40, 107]$ in order to keep predominantly the monotonic behavior of (normalized) counts $f_{i,j}$ at the right tails. Of course, the smoothed data can be further analyzed using methods of functional data analysis [18], adapted in order to respect specific properties of densities. It is demonstrated here for case of the compositional functional principal component analysis (SFPCA) [9]. This statistical tool has been recently designed based on the Bayes space methodology,



(a) Example of smoothed raw density data in \mathcal{B}^2 (left) and L_0^2 (right) spaces.



(b) Smoothed raw density data in \mathcal{B}^2 (left) and L_0^2 (right) spaces.

Figure 15: Smoothed weight density functions via compositional smoothing splines in \mathcal{B}^2 space and its clr transformation in L_0^2 (right) spaces. Data are displayed on blue scale distinguishing age groups: with increasing age, the intensity of blue color increases. Vertical dashed gray lines indicate knots position.

so it enables to capture the main modes of *relative* variability in a data set consisting of sampled density functions. Given a data set of N zero-mean functional observations X_1, \dots, X_N in $\mathcal{B}^2(I)$, SFPCA aims to find the (normalized and orthogonal) directions of maximum variability in dataset, i.e., a collection of density functions $\{\theta_\kappa\}_{\kappa \geq 1}$ called simplicial functional principal components (SPFCs) which maximize the following objective function over $\theta \in \mathcal{B}^2(I)$,

$$\sum_{i=1}^N \langle X_i, \theta \rangle_{\mathcal{B}}^2 \text{ subject to } \|\theta\|_{\mathcal{B}} = 1; \text{ with } \quad \langle \theta, \theta_\kappa \rangle_{\mathcal{B}} = 0, \kappa < K, \quad (27)$$

where the orthogonality condition is assumed to be fulfilled for $K \geq 2$. Since $\langle X_i, \theta \rangle_{\mathcal{B}}$ represents a projection of X_i along the direction $\theta \in \mathcal{B}^2(I)$, in fact we look for orthogonal basis functions in $\mathcal{B}^2(I)$ maximizing the relative variability of these projections. The maximization task (27) is efficiently implemented by applying the clr transformation (3) and the output can be back-transformed from the $L^2(I)$ to the $\mathcal{B}^2(I)$ space, as detailed in [9].

The interpretation of SFPCs can be performed by displaying:

- individual SFPCs (as clr transformed density functions, SFPCs always represent contrasts between the parts of domain I);
- overall mean density function \bar{X} along with its perturbation by SFPCs powered by a suitable constant,

$$\bar{X} \oplus \sqrt{\rho_\kappa} \odot \theta_\kappa, \quad \bar{X} \ominus \sqrt{\rho_\kappa} \odot \theta_\kappa, \quad (28)$$

where ρ_κ is an amount of the variability of the dataset along the direction x_κ and it holds $\rho_1 \geq \rho_2 \geq \dots$. This is a natural choice because SFPCs represent variation around the overall mean density function;

- the projection of dataset along the directions θ_κ ,

$$\langle X_i, \theta_\kappa \rangle_{\mathcal{B}} \odot \theta_\kappa = x_{i\kappa} \odot \theta_\kappa, \quad i = 1, \dots, N,$$

where $x_{i\kappa} = \langle X_i, \theta_\kappa \rangle_{\mathcal{B}}, i = 1, \dots, N$ are so called principal component scores associated with the κ th SFPCs θ_κ . The scores can be plotted for pairs of the first SFPCs to assess the relationship among sampled density functions or to reveal presence of outlying observations;

- to complete the above interpretation it is important to note that the original functions X_1, \dots, X_N and the eigenfunctions $\theta_\kappa, \kappa \geq 1$ are based on a CB -spline basis expansion

$$X_i(\cdot) = \bigoplus_{\nu=-3}^1 c_{i,\nu} \odot \zeta_\nu(\cdot), \quad \theta_\kappa(\cdot) = \bigoplus_{\nu=-3}^1 b_{\kappa,\nu} \odot \zeta_\nu(\cdot), \quad (29)$$

respectively, by considering (26).

SFPCA is also a statistical method for reducing dimensionality of dataset. The number of SFPCs can be determined from the scree plot which displays cumulative percentage of the total variance explained by each subsequent SFPC. That is, the dimensionality is identified by a point in scree plot at which explained variability drops off.

For the actual computation, CB -splines (29) of the input functional observations, represented by the corresponding ZB -splines (26), were expressed by B -splines with B -spline coefficients (listed in Table 4) using formula (16). The output of SFPCA for body weight density functions is reported in Figure 16. According to scree plot (Figure 16b), two or three SFPCs should be taken, but we resort to use only first two of them which capture together almost 85% of the total variability of the data set. The first SFPC (Figure 16c) represents the contrast between the weight below and above 78 kg, which could be considered as a reference (average) weight. Hence, higher scores along the SFPC₁ are expected for age groups with higher incidence of individuals with higher body weight than the average, and, conversely, lower scores are associated with age groups with higher incidence of individuals with lower body weight than the average. The interpretation of SFPC₁ can be obviously linked with age, see Figure 16b. The scree plot more or less separates rather

Table 1: Histogram data for four age groups: $[15, 16)$, $[22, 23)$, $[23, 24)$ and $[30, 31)$. \mathbf{f}_i are raw density values at midpoints $\mathbf{t}_i = (t_{i,1}, \dots, t_{i,q_i})^\top$ of weight classes with proportions \mathbf{p}_i for $i = 1, 8, 9, 16$; q_i indicates the number of the weight classes.

[15, 16)	\mathbf{p}_1	0.0656	0.2625	0.3375	0.2156	0.0750	0.0281	0.0094	0.0062			$q_1 = 8$
	\mathbf{f}_1	0.0075	0.0300	0.0386	0.0246	0.0086	0.0032	0.0011	0.0007			
	\mathbf{t}_1	44.375	53.125	61.875	70.625	79.375	88.125	96.875	105.625			
[22, 23)	\mathbf{p}_8	0.0156	0.0869	0.1804	0.2138	0.2272	0.1514	0.0935	0.0200	0.0067	0.0045	$q_8 = 10$
	\mathbf{f}_8	0.0022	0.0124	0.0258	0.0305	0.0325	0.0216	0.0134	0.0029	0.0010	0.0006	
	\mathbf{t}_8	43.5	50.5	57.5	64.5	71.5	78.5	85.5	92.5	99.5	106.5	
[23, 24)	\mathbf{p}_9	0.0078	0.0908	0.2100	0.1971	0.1659	0.1659	0.1011	0.0259	0.0337	0.0017	$q_9 = 10$
	\mathbf{f}_9	0.0011	0.0130	0.0300	0.0282	0.0237	0.0237	0.0144	0.0037	0.0048	0.0002	
	\mathbf{t}_9	43.5	50.5	57.5	64.5	71.5	78.5	85.5	92.5	99.5	106.5	
[30, 31)	\mathbf{p}_{16}	0.0568	0.1023	0.2045	0.2386	0.2159	0.1364	0.0455			$q_{16} = 7$	
	\mathbf{f}_{16}	0.0057	0.0102	0.0205	0.0239	0.0216	0.0136	0.0045				
	\mathbf{t}_{16}	45.0	55.0	65.0	75.0	85.0	95.0	105.0				

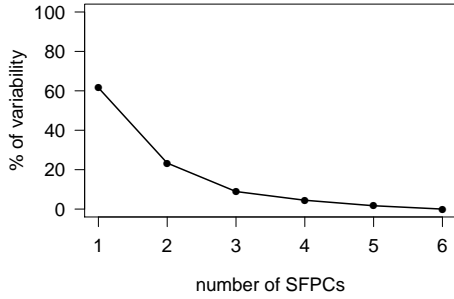
right skewed weight density functions of younger age groups (located on the left in the scree plot) from those more symmetric ones associated with older age groups (located on the right in the scree plot).

The second SFPC (Figure 16d) characterizes the variability within the tails of density functions, i.e. the main contribution to the variability along SFPC₂ is provided by the lowest and highest weight values (≤ 51 kg and ≥ 98 kg respectively). It contrasts low and high weights (associated with high scores along the SFPC₂) against middle weight values (associated with low scores along the SFPC₂), see Figure 16b. The consistent interpretation can be also observed from Figure 16e which displays the variation along the first two directions – SFPC₁ and SFPC₂ – with respect to sample mean $\bar{f}(t), t \in I$ (i.e. $\bar{f} \oplus / \ominus 2\sqrt{\rho_\kappa} \odot \text{SFPC}_\kappa, \kappa = 1, 2$).

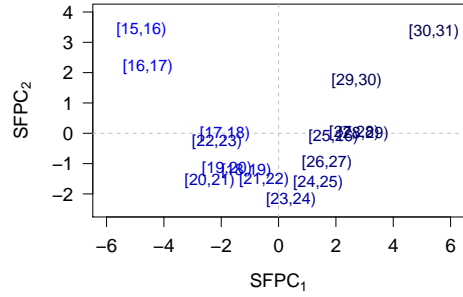
Figures 16f and 16g, respectively, represent two main modes of variability in the data set $(\langle f_i, \theta_\kappa \rangle_{\mathcal{B}} \odot \theta_\kappa, \kappa = 1, 2, i = 1, \dots, N)$. For instance, the variation along SFPC₂ is confirmed to be exhibited in tails of density functions and the observations with lowest (gold curve) and highest score (red curve) further support the conclusions made so far. The high scores along the second direction thus reflect heavier tails and, conversely, the low scores along the second direction reflects low incidence of individuals with *extreme* (both small and high) weights. Nevertheless, the relationship of scores (Figure 16b) is apparent: at the beginning, they continue to fall, reach a bottom and then continue to grow. The relationship might be partially explained by unequal representation of men and women in age groups and unequal number of observations in these age groups. Another reason might be that data corresponding to age groups with low SFPC₂ scores were collected mostly from students of the Faculty of Physical Culture at Palacký University in Olomouc, Czech Republic, which form more homogeneous population than an average one. In any case, the second SFPC reveals an interesting feature which is worth to be further investigated.

7 Conclusions

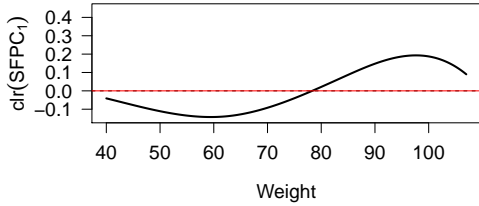
The compositional splines, which enable to construct a spline basis in the clr space of density functions (*ZB*-spline basis) and consequently also in the original space of densi-



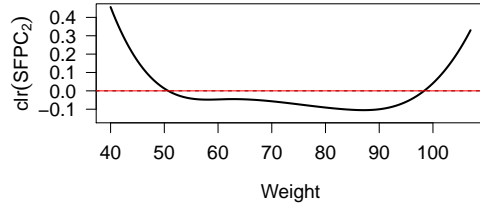
(a) Explained variability.



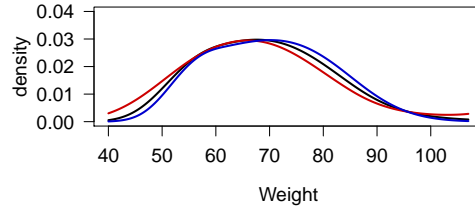
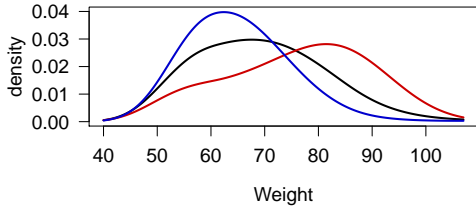
(b) Scores for SFPC₁ and SFPC₂.



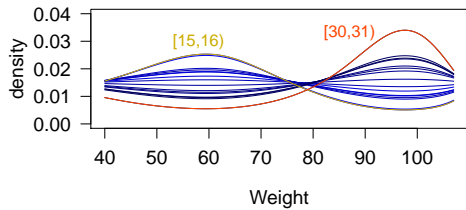
(c) SFPC₁ (61.6% of variability).



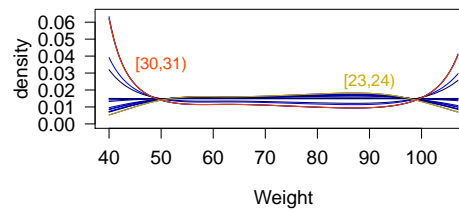
(d) SFPC₂ (23.3% of variability).



(e) Variability around the mean weight density function ($\bar{f} \oplus / \ominus 2\sqrt{\rho_\kappa} \odot \text{SFPC}_\kappa, \kappa = 1, 2$).



(f) Projection using only SFPC₁.



(g) Projection using only SFPC₂.

Figure 16: SFPCA results for weight density functions. In panel (e), the red curve indicates adding (\oplus) of $2\sqrt{\rho_\kappa}$ multiple of SFPC _{κ} and the blue curve indicates subtracting (\ominus) of $2\sqrt{\rho_\kappa}$ multiple of SFPC _{ν} to the overall mean weight density function $\bar{f}(t), t \in I$, indicated by the black curve (left: $\kappa = 1$ and right: $\kappa = 2$, respectively); ρ_κ is the standard deviation along SFPC _{κ} , $\kappa = 1, 2$.

Table 2: Input data for smoothing procedure: $\text{clr}(\mathbf{f}_i)$ are raw clr density values at mid-points $\mathbf{t}_i = (t_{i,1}, \dots, t_{i,q_i})^\top$ of the weight classes for $i = 1, 2, \dots, N$; q_i indicates the number of the weight classes.

[15, 16)	$\text{clr}[\mathbf{f}_1]$ \mathbf{t}_1	0.100 44.375	1.486 53.125	1.737 61.875	1.289 70.625	0.233 79.375	-0.748 88.125	-1.846 96.875	-2.252 105.625		$q_1 = 8$	
[16, 17)	$\text{clr}[\mathbf{f}_2]$ \mathbf{t}_2	-0.210 44.375	1.217 53.125	1.760 61.875	1.636 70.625	0.396 79.375	-0.392 88.125	-2.001 96.875	-2.407 105.625		$q_2 = 8$	
[17, 18)	$\text{clr}[\mathbf{f}_3]$ \mathbf{t}_3	-1.375 43.889	0.570 51.667	1.316 59.444	1.669 67.222	1.381 75.000	0.534 82.778	-0.364 90.556	-2.069 98.333	-1.663 106.111	$q_3 = 9$	
[18, 19)	$\text{clr}[\mathbf{f}_4]$ \mathbf{t}_4	-1.354 43.5	0.592 50.5	1.419 57.5	1.443 64.5	1.406 71.5	1.131 78.5	0.563 85.5	-0.661 92.5	-1.171 99.5	-3.369 106.5	$q_4 = 10$
[19, 20)	$\text{clr}[\mathbf{f}_5]$ \mathbf{t}_5	-1.536 43.5	0.628 50.5	1.408 57.5	1.555 64.5	1.535 71.5	1.209 78.5	0.302 85.5	-0.774 92.5	-1.536 99.5	-2.789 106.5	$q_5 = 10$
[20, 21)	$\text{clr}[\mathbf{f}_6]$ \mathbf{t}_6	-1.341 43.5	0.674 50.5	1.333 57.5	1.558 64.5	1.638 71.5	1.452 78.5	0.422 85.5	-0.568 92.5	-2.034 99.5	-3.133 106.5	$q_6 = 10$
[21, 22)	$\text{clr}[\mathbf{f}_7]$ \mathbf{t}_7	-1.746 43.5	0.451 50.5	1.185 57.5	1.463 64.5	1.411 71.5	1.131 78.5	0.531 85.5	-0.242 92.5	-1.746 99.5	-2.439 106.5	$q_7 = 10$
[22, 23)	$\text{clr}[\mathbf{f}_8]$ \mathbf{t}_8	-1.168 43.5	0.550 50.5	1.281 57.5	1.450 64.5	1.511 71.5	1.106 78.5	0.624 85.5	-0.917 92.5	-2.015 99.5	-2.421 106.5	$q_8 = 10$
[23, 24)	$\text{clr}[\mathbf{f}_9]$ \mathbf{t}_9	-1.884 43.5	0.573 50.5	1.412 57.5	1.348 64.5	1.177 71.5	1.177 78.5	0.681 85.5	-0.680 92.5	-0.417 99.5	-3.388 106.5	$q_9 = 10$
[24, 25)	$\text{clr}[\mathbf{f}_{10}]$ \mathbf{t}_{10}	-1.602 43.889	0.595 51.667	1.186 59.444	1.274 67.222	1.106 75.000	0.796 82.778	0.056 90.556	-0.423 98.333	-2.988 106.111		$q_{10} = 9$
[25, 26)	$\text{clr}[\mathbf{f}_{11}]$ \mathbf{t}_{11}	-1.401 43.889	0.471 51.667	0.768 59.444	0.824 67.222	1.145 75.000	0.850 82.778	0.209 90.556	-1.178 98.333	-1.688 106.111		$q_{11} = 9$
[26, 27)	$\text{clr}[\mathbf{f}_{12}]$ \mathbf{t}_{12}	-1.045 44.375	0.513 53.125	0.901 61.875	1.180 70.625	1.258 79.375	0.513 88.125	-0.485 96.875	-2.836 105.625			$q_{12} = 8$
[27, 28)	$\text{clr}[\mathbf{f}_{13}]$ \mathbf{t}_{13}	-0.816 44.375	0.570 53.125	0.742 61.875	0.742 70.625	1.056 79.375	0.570 88.125	-0.256 96.875	-2.608 105.625			$q_{13} = 8$
[28, 29)	$\text{clr}[\mathbf{f}_{14}]$ \mathbf{t}_{14}	-1.155 45.0	0.579 55.0	0.790 65.0	0.965 75.0	0.690 85.0	-0.308 95.0	-1.561 105.0				$q_{14} = 7$
[29, 30)	$\text{clr}[\mathbf{f}_{15}]$ \mathbf{t}_{15}	-1.060 45.0	0.480 55.0	0.837 65.0	0.674 75.0	0.614 85.0	-0.773 95.0	-0.773 105.0				$q_{15} = 7$
[30, 31)	$\text{clr}[\mathbf{f}_{16}]$ \mathbf{t}_{16}	-0.756 45.0	-0.168 55.0	0.525 65.0	0.679 75.0	0.579 85.0	0.120 95.0	-0.979 105.0				$q_{16} = 7$

Table 3: ZB -spline coefficients for clr transformed density functions of $N = 16$ age groups.

age group	spline coefficients, $\mathbf{z}_i = (z_{i,-3}, \dots, z_{i,1})^\top, i = 1, \dots, N$				
[15, 16)	-6.950	6.647	46.536	40.973	13.163
[16, 17)	-7.806	-0.596	41.616	45.181	14.083
[17, 18)	-16.677	-11.292	18.284	43.917	9.102
[18, 19)	-17.067	-8.988	21.373	33.533	20.188
[19, 20)	-18.483	-9.902	22.408	38.249	16.447
[20, 21)	-17.242	-7.010	18.199	46.788	18.682
[21, 22)	-20.452	-10.875	11.653	36.887	14.797
[22, 23)	-15.236	-5.368	16.735	46.421	14.071
[23, 24)	-22.485	-12.348	17.033	23.450	20.153
[24, 25)	-19.873	-14.176	13.567	20.115	19.448
[25, 26)	-19.011	-5.949	-4.623	30.860	9.973
[26, 27)	-14.997	-10.545	2.638	28.225	19.143
[27, 28)	-14.461	-4.455	-0.689	21.892	18.070
[28, 29)	-18.518	-11.045	-2.723	21.744	10.395
[29, 30)	-16.445	-9.417	-1.814	23.562	2.889
[30, 31)	-5.077	-15.534	-4.171	8.220	7.618

Table 4: B -spline coefficients for clr transformed density functions of $N = 16$ age groups.

age group	spline coefficients, $\mathbf{b}_i = (b_{i,-3}, \dots, b_{i,2})^\top, i = 1, \dots, N$					
[15, 16)	-1.264	1.236	2.381	-0.332	-2.472	-2.289
[16, 17)	-1.419	0.655	2.520	0.213	-2.764	-2.449
[17, 18)	-3.032	0.490	1.766	1.530	-3.095	-1.583
[18, 19)	-3.103	0.734	1.813	0.726	-1.186	-3.511
[19, 20)	-3.361	0.780	1.929	0.946	-1.938	-2.860
[20, 21)	-3.135	0.930	1.505	1.707	-2.498	-3.249
[21, 22)	-3.719	0.871	1.345	1.507	-1.964	-2.573
[22, 23)	-2.770	0.897	1.320	1.772	-2.876	-2.447
[23, 24)	-4.088	0.922	1.754	0.383	-0.293	-3.505
[24, 25)	-3.613	0.518	1.656	0.391	-0.059	-3.382
[25, 26)	-3.456	1.187	0.079	2.118	-1.857	-1.734
[26, 27)	-2.727	0.405	0.787	1.528	-0.807	-3.329
[27, 28)	-2.629	0.910	0.225	1.348	-0.340	-3.143
[28, 29)	-3.367	0.679	0.497	1.461	-1.009	-1.808
[29, 30)	-2.990	0.639	0.454	1.515	-1.838	-0.502
[30, 31)	-0.923	-0.951	0.678	0.740	-0.053	-1.325

ties (CB -spline basis), might become an important contribution within the Bayes space methodology for processing of functional data carrying relative information. They provide a solid theoretical base for further developments of the approximation theory in context of the Bayes spaces, but even more importantly, compositional splines can be used also for adaptation of popular methods of functional data analysis for density functions. Here the case of compositional functional principal component analysis was presented, but similarly, e.g., regression analysis or classification methods could be developed. Also further tuning of the compositional splines is possible, here represented by the smoothing compositional splines or by orthonormalization of the ZB -basis. The latter case be used for an orthogonal projection of a density function on a subset of CB -splines, to further applications within the approximation theory or also for development of the theoretical framework of functional data analysis.

The pending challenge is to generalize the methodology introduced above also to p -dimensional density functions, $p > 1$, which can be formally extended from any univariate density $f(x)$, $x \in I = [a, b]$ to $f(\mathbf{x})$, where $\mathbf{x} = (x_1, \dots, x_p)^\top \in \mathcal{I} = I_1 \times \dots \times I_p = [a_1, b_1] \times \dots \times [a_p, b_p]$, in Equations (1) to (6); $\eta = b - a$ would be replaced by $H = \prod_{i=1}^p (b_i - a_i)$. Currently an approach which focuses on keeping the zero integral constraint of the clr transformed densities was developed in [8] as a generalization of [12], which, however, does not lead to a compositional counterpart of the B -spline basis. A consistent approach in this direction is currently under development.

Acknowledgements

The authors gratefully acknowledge both the support by Czech Science Foundation GA18-09188S, the grant IGA_PrF_2018_024 Mathematical Models of the Internal Grant Agency of the Palacký University in Olomouc, and the grant COST Action CRoNoS IC1408.

References

- [1] J. Aitchison. The statistical analysis of compositional data. *Journal of the Royal Statistical Society. Series B (Methodological)*, pages 139–177, 1982.
- [2] C. De Boor. *A practical guide to splines*, volume 27. Springer-Verlag New York, 1978.
- [3] P. Delicado. Dimensionality reduction when data are density functions. *Computational Statistics & Data Analysis*, 55(1):401–420, 2011.
- [4] P. Dierckx. *Curve and surface fitting with splines*. Oxford University Press, 1995.
- [5] M. L. Eaton. Multivariate statistics: a vector space approach. *JOHN WILEY & SONS, INC., 605 THIRD AVE., NEW YORK, NY 10158, USA, 1983, 512*, 1983.
- [6] J. J. Egozcue, J. L. Díaz-Barrero, and V. Pawlowsky-Glahn. Hilbert space of probability density functions based on aitchison geometry. *Acta Mathematica Sinica*, 22(4):1175–1182, 2006.
- [7] J. J. Egozcue, V. Pawlowsky-Glahn, G. Mateu-Figueras, and C. Barcelo-Vidal. Isometric logratio transformations for compositional data analysis. *Mathematical Geology*, 35(3):279–300, 2003.
- [8] D. Guégan and M. Iacopini. Nonparametric forecasting of multivariate probability density functions. *arXiv preprint arXiv:1803.06823*, 2018.
- [9] K. Hron, A. Menafoglio, M. Templ, K. Hruzová, and P. Filzmoser. Simplicial principal component analysis for density functions in bayes spaces. *Computational Statistics & Data Analysis*, 94:330–350, 2016.
- [10] J. Machalová. Optimal interpolating and optimal smoothing spline. *Journal of Electrical Engineering*, 53:79–82, 2002.
- [11] J. Machalová. Optimal interpolatory splines using b -spline representation. *Acta Universitatis Palackianae Olomucensis. Facultas Rerum Naturalium. Mathematica*, 41(1):105–118, 2002.
- [12] J. Machalova, K. Hron, and G. S. Monti. Preprocessing of centred logratio transformed density functions using smoothing splines. *Journal of Applied Statistics*, 43(8):1419–1435, 2016.
- [13] J.-A. Martín-Fernández, K. Hron, M. Templ, P. Filzmoser, and J. Palarea-Albaladejo. Bayesian-multiplicative treatment of count zeros in compositional data sets. *Statistical Modelling*, 15(2):134–158, 2015.
- [14] A. Menafoglio, A. Guadagnini, and P. Secchi. A kriging approach based on aitchison geometry for the characterization of particle-size curves in heterogeneous aquifers. *Stochastic Environmental Research and Risk Assessment*, 28(7):1835–1851, 2014.

- [15] A. Menafoglio, A. Guadagnini, and P. Secchi. Stochastic simulation of soil particle-size curves in heterogeneous aquifer systems through a bayes space approach. *Water Resources Research*, 52(8):5708–5726, 2016.
- [16] V. Pawlowsky-Glahn and J. J. Egozcue. Geometric approach to statistical analysis on the simplex. *Stochastic Environmental Research and Risk Assessment*, 15(5):384–398, 2001.
- [17] V. Pawlowsky-Glahn, J. J. Egozcue, and R. Tolosana-Delgado. *Modeling and analysis of compositional data*. John Wiley & Sons, 2015.
- [18] J. Ramsay. Functional data analysis. *Encyclopedia of Statistics in Behavioral Science*, 2005.
- [19] A. Redd. A comment on the orthogonalization of b-spline basis functions and their derivatives. *Statistics and Computing*, 22(1):251–257, 2012.
- [20] R. Talská, A. Menafoglio, J. Machalová, K. Hron, and E. Fišerová. Compositional regression with functional response. *Computational Statistics & Data Analysis*, 123:66–85, 2018.
- [21] K. G. Van den Boogaart, J. J. Egozcue, and V. Pawlowsky-Glahn. Bayes linear spaces. *SORT: statistics and operations research transactions, 2010, vol. 34, núm. 4, p. 201-222*, 2010.
- [22] K. G. Van den Boogaart, J. J. Egozcue, and V. Pawlowsky-Glahn. Bayes hilbert spaces. *Australian & New Zealand Journal of Statistics*, 56(2):171–194, 2014.